# Spin–orbit perturbations between the $A(2)^1\Sigma^+$ and $b(1)^3\Pi_0$ states of NaK

Hongqiao Sun and John Huennekens
*Department of Physics, Lehigh University, Bethlehem, Pennsylvania 18015*

(Received 24 February 1992; accepted 1 June 1992)

We have studied spin–orbit perturbations between the $A(2)\ ^1\Sigma^+$ and $b(1)\ ^3\Pi_0$ states of the NaK molecule by accurately measuring the energies of mutually perturbing levels, and by measuring ratios of $A(2)\ ^1\Sigma^+ \rightarrow X(1)\ ^1\Sigma^+$ and $b(1)\ ^3\Pi_0 \rightarrow a(1)\ ^3\Sigma^+$ emission intensities, for five perturbed pairs. This allows two partially independent determinations of each perturbation matrix element $|\langle 1\ ^3\Pi_0(v_t',J')|\hat{H}_{so}|2^1\Sigma^+(v_s',J')\rangle|$. From these matrix elements, and calculated vibrational overlap integrals $\langle v_t'|v_s'\rangle$, the electronic part of the perturbation matrix element, $H_{el} \equiv |\langle 1\ ^3\Pi_0(v_t',J')|\hat{H}_{so}|2\ ^1\Sigma^+(v_s',J')\rangle|/|\langle v_t'|v_s'\rangle|$, was obtained. Our results for $H_{el}$ from the two methods are consistent, and independent of vibrational and rotational quantum numbers, as expected. The determined best value for $H_{el}$ is $(15.64 \pm 0.39)\ \mathrm{cm}^{-1}$.

## I. INTRODUCTION

Singlet states of alkali diatomic molecules have been studied extensively using the full range of high-resolution laser spectroscopic techniques (for example, see Ref. 1 for a review of data on $Na_2$ and Ref. 2 for an excellent summary of the current state of knowledge concerning $Cs_2$). However, while singlet states couple to the $X(1)\ ^1\Sigma^+$ ground state through some number of dipole-allowed transitions, the $\Delta S=0$ selection rule makes the triplet states more difficult to study. In recent years this situation has changed with the advent of the perturbation-facilitated optical–optical double-resonance technique.[3–5] Thus spin–orbit perturbations between singlet and triplet states of alkali molecules create pathways into the triplet manifolds, allowing researchers to map out many of these triplet states. Moreover, the fact that the lowest triplet state of all alkali diatomic molecules, $1\ ^3\Sigma^+$, is repulsive, means that triplet bands terminating on this state are continuous. It has therefore been suggested that this "excimerlike" nature of these triplet bands may be used for developing high-power, tunable, near-infrared lasers.[6]

Spin–orbit perturbations between the alkali $A\ ^1\Sigma^+$ and $b\ ^3\Pi$ states are also of interest since they contribute to collisional excitation transfer from one fine-structure level to another,[7–9]

$$A(^2P_{3/2})+B(^2S_{1/2}) \rightleftharpoons A(^2P_{1/2})+B(^2S_{1/2}). \qquad (1)$$

Here $A(^2P_{3/2})$ and $A(^2P_{1/2})$ represent alkali atoms in the $J=\frac{3}{2}$ and $J=\frac{1}{2}$ fine-structure levels, respectively, of the first excited state, and $B(^2S_{1/2})$ is a ground-state alkali atom of the same or a different species. In the light alkalis, this excitation transfer process is dominated by long-range Coriolis interactions.[9] However, for heavier alkalis such as cesium, this process is dominated by the $A\ ^1\Sigma^+$–$1\ ^3\Pi_0$ spin–orbit interaction. In this latter case, the value of the spin–orbit interaction strength is significant, because the excitation transfer process [Eq. (1)] limits the performance of ultracold cesium traps. These traps are currently produced by laser cooling techniques utilizing diode lasers *tuned* to the $6S_{1/2} \rightarrow 6P_{3/2}$ transition. In this case, excited $6P_{3/2}$ atoms colliding with ground-state atoms can interact along the $1\ ^3\Pi_0$ potential, switch over to the $A\ ^1\Sigma^+$ potential (due to the spin–orbit interaction), and dissociate to the $6\ ^2P_{1/2}$ limit, gaining $554\ \mathrm{cm}^{-1}$ of kinetic energy in the process. This additional kinetic energy is sufficient to cause these atoms to leave the trap.

The $A\ ^1\Sigma^+$–$1\ ^3\Pi_0$ spin–orbit perturbations have been extensively studied for the homonuclear alkali molecules.[4,5,10–19] Because the perturbations between bound molecular states cause rovibrational spectral lines to shift from their unperturbed positions, which are defined by empirical (deperturbed) energy expressions, a common method of studying the spin–orbit perturbation effects is high-resolution spectroscopy.[12–16,18] Also, $A\ ^1\Sigma^+$–$1\ ^3\Pi_0$ perturbations can be explored by studying altered properties, such as anomalous lifetimes or line intensities associated with perturbed levels.[4,5,17,19] These spin–orbit perturbation parameters have been reported for the $Li_2$,[4,5] $Na_2$,[13,16,17,19] and $K_2$ (Ref. 18) molecules. In this paper we report the perturbation parameter for the analogous $A(2)\ ^1\Sigma^+$–$1\ ^3\Pi_0$ spin–orbit perturbation of NaK, the first such measurement for a heteronuclear alkali molecule. The heteronuclears are of particular interest because the $1\ ^3\Pi_0 \rightarrow 1\ ^3\Sigma^+$ transitions are allowed, whereas the analogous $1\ ^3\Pi_u \rightarrow 1\ ^3\Sigma_u^+$ bands of the homonuclears are forbidden by the $u \leftarrow | \rightarrow u$ symmetry selection rule. In our experiment, the NaK $b(1)\ ^3\Pi_0$–$A(2)\ ^1\Sigma^+$ spin–orbit perturbation strength is determined by accurately measuring the energies of pairs of perturbed levels, and by measuring the ratio of the $b(1)\ ^3\Pi_0 \rightarrow a(1)\ ^3\Sigma^+$ bound–free emission intensity to the $A(2)\ ^1\Sigma^+ \rightarrow X(1)\ ^1\Sigma^+$ bound–bound emission intensity for each member of the same pairs of perturbed levels.

In NaK the $1\ ^3\Pi_\Omega$ and $2\ ^1\Sigma^+$ states both dissociate to the sodium $3s$ plus potassium $4p$ atomic state limit, and these two potentials overlap significantly (see Fig. 1). The spin–orbit perturbation between nearby singlet and triplet levels of the same $J$ results in perturbed levels with properties that are mixtures of those of the pure $1\ ^3\Pi$ and $2\ ^1\Sigma^+$ levels.[20–23] Therefore we can directly excite NaK molecules from a single rovibrational level of the ground state, $1\ ^1\Sigma^+$, to a specific perturbed upper state, by using a tunable, narrow-bandwidth, single-mode cw dye laser.[23]

 0021-9606/92/194714-09$006.00 © 1992 American Institute of Physics

Downloaded 27 Feb 2001 to 128.180.23.36. Redistribution subject to AIP copyright, see http://ojps.aip.org/jcpo/jcpcpyrts.html

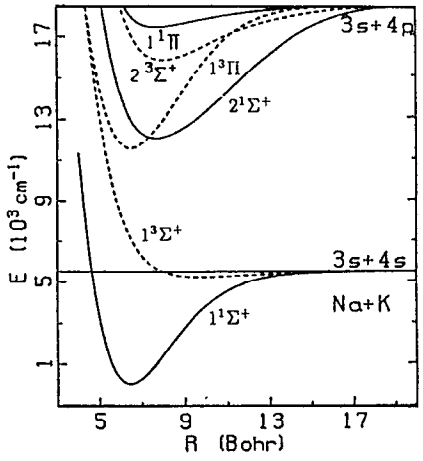


FIG. 1. Lowest six NaK molecular potential curves (from Ref. 33). Throughout the text, the notation $2\,^1\Sigma^+$ refers to the second-lowest $^1\Sigma^+$ state, etc. This replaces the older notation in which states were labeled by letters (i.e., $X\,^1\Sigma^+ = 1\,^1\Sigma^+$, $A\,^1\Sigma^+ = 2\,^1\Sigma^+$, $a\,^3\Sigma^+ = 1\,^3\Sigma^+$, $b\,^3\Pi = 1\,^3\Pi$).

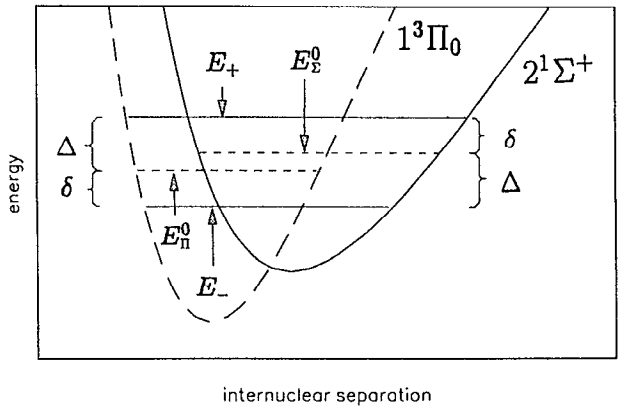


FIG. 2. Schematic diagram showing one pair of perturbed levels (solid lines) and the corresponding unperturbed levels (dashed lines). In this case we assume that the unperturbed singlet lies higher.

We detect these perturbed levels by simultaneous observation of bound–bound ($2\,^1\Sigma^+ \rightarrow 1\,^1\Sigma^+$) and bound–free ($1\,^3\Pi_0 \rightarrow 1\,^3\Sigma^+$) emissions. The analysis of the spin–orbit $2\,^1\Sigma^+ - 1\,^3\Pi_0$ perturbations relies heavily on previous experimental determinations of the bound $1\,^3\Pi_1$, $1\,^1\Sigma^+$, and $2\,^1\Sigma^+$ potentials of NaK which were accurately mapped using high-resolution Fourier-transform spectroscopy.[24–26]

## II. THEORETICAL ANALYSIS

In the specific case under consideration in this paper, the spin–orbit perturbation only occurs between levels of the $1\,^3\Pi_0$ and $2\,^1\Sigma^+$ states because of the $\Delta\Omega=0$ spin–orbit perturbation selection rule.[11,13,27] The $1\,^3\Pi_2(v_t',J')$ and $1\,^3\Pi_1(v_t',J')$ levels also couple to the $1\,^3\Pi_0(v_t',J')$ and $2\,^1\Sigma^+(v_s',J')$ levels through second-order spin–orbit effects[27] ($\Delta J=0$ is still a strict selection rule for this type of perturbation as well). Thus in the general case, a $4\times4$ perturbation matrix must be solved. However, if we study sets of levels in which the $2\,^1\Sigma^+(v_s',J')$ lies closest to the $1\,^3\Pi_0(v_t',J')$, and neglect the weaker second-order effects, the problem reduces to a two-state system. (Later in this paper we will introduce a small correction term to account for the rotational mixing within the $^3\Pi_\Omega$ manifold; i.e., to account for the fact that the "unperturbed" $^3\Pi_0$ level actually contains small admixtures of $^3\Pi_1$ and $^3\Pi_2$ character.)

Under these conditions, the interaction matrix can be written as[20]

$$\begin{pmatrix} E_\Sigma^0 - E & H_{\Sigma\Pi} \\ H_{\Pi\Sigma} & E_\Pi^0 - E \end{pmatrix} \begin{pmatrix} a \\ b \end{pmatrix} = 0, \tag{2}$$

where the column vector $\binom{a}{b}$ represents the perturbed state wave function

$$a|2\,^1\Sigma^+(v_s',J')\rangle + b|1\,^3\Pi_0(v_t',J')\rangle, \tag{3}$$

and $|2\,^1\Sigma^+(v_s',J')\rangle$ and $|1\,^3\Pi_0(v_t',J')\rangle$ are the unperturbed level wave functions. Therefore, $a$ and $b$ are the mixing amplitude coefficients. In the energy matrix, $E_\Sigma^0$ and $E_\Pi^0$ are the energies of the unperturbed $2\,^1\Sigma^+$ and $1\,^3\Pi_0$ levels, respectively. The spin–orbit perturbation matrix element $|H_{so}|$ is defined as

$$\begin{aligned} |H_{so}| &= |H_{\Sigma\Pi}| \\ &= |H_{\Pi\Sigma}| \\ &= |\langle 2\,^1\Sigma^+(v_s',J')|\hat{H}_{so}|1\,^3\Pi_0(v_t',J')\rangle|. \end{aligned} \tag{4}$$

The perturbed state energies $E_\pm$, found by setting the determinant of the $2\times2$ energy matrix in Eq. (2) equal to 0, are given by

$$E_\pm = \tfrac{1}{2}\{(E_\Sigma^0 + E_\Pi^0) \pm [(E_\Sigma^0 - E_\Pi^0)^2 + 4|H_{so}|^2]^{1/2}\}. \tag{5}$$

The specific perturbed state wave functions $\phi_1$ and $\phi_2$, which are solutions to Eq. (2), are given by

$$\phi_1 = A|2\,^1\Sigma^+(v_s',J')\rangle + B|1\,^3\Pi_0(v_t',J')\rangle \tag{6}$$

and

$$\phi_2 = B|2\,^1\Sigma^+(v_s',J')\rangle - A|1\,^3\Pi_0(v_t',J')\rangle. \tag{7}$$

Using the normalization condition $A^2 + B^2 = 1$, the mixing coefficients are easily found to be

$$A = \frac{|H_{so}|}{(\delta^2 + |H_{so}|^2)^{1/2}} \tag{8}$$

and

$$B = \frac{\delta}{(\delta^2 + |H_{so}|^2)^{1/2}}. \tag{9}$$

Here we have defined the energy shifts $\delta \equiv E_+ - E_\Sigma^0 = E_\Pi^0 - E_-$ and $\Delta \equiv E_+ - E_\Pi^0 = E_\Sigma^0 - E_-$ as the splittings of the perturbed and unperturbed levels (see Fig. 2) and we have assumed that $\delta$ is the smaller energy shift ($\delta < \Delta$) as depicted in Fig. 2. (Note that if the unperturbed triplet lies above the unperturbed singlet, then $\delta \equiv E_+ - E_\Pi^0 = E_\Sigma^0 - E_-$ and $\Delta \equiv E_+ - E_\Sigma^0 = E_\Pi^0 - E_-$.)


Downloaded 27 Feb 2001 to 128.180.23.36. Redistribution subject to AIP copyright, see http://ojps.aip.org/jcpo/jcpcpyrts.html

From Eq. (5), it is clear that $H_{so}$ can be determined from any three of the four quantities $E_+$, $E_-$, $E^0_\Sigma$, and $E^0_\Pi$. In particular, it can be shown that

$$|H_{so}| = \sqrt{\Delta\delta}. \tag{10}$$

Conversely, $|H_{so}|$ can be determined from the amplitude ratio and the energy shift; i.e.,

$$|H_{so}| = \delta A/B. \tag{11}$$

In our experiment, $E_+$ and $E_-$ can be determined accurately by precise measurement of the laser frequencies required to pump the NaK molecule from one specific level of the ground ($1\,^1\Sigma^+$) state to each of these two perturbed levels, respectively. We obtain the unperturbed $2\,^1\Sigma^+$ levels ($E^0_\Sigma$) from the experimental constants of Ross and coworkers[26] for that state. Using these three values, we can obtain $|H_{so}|$ from Eq. (10). The unperturbed $1\,^3\Pi_0$ level energies can be derived from the accurate $1\,^3\Pi_1$ constants of Ref. 24 and the splittings of levels in the various $1\,^3\Pi_\Omega$ states suggested in that same reference,

$$E^0[1\,^3\Pi_0(v_t',J')] = E^0[1\,^3\Pi_1(v_t',J')] - 15.557\ \text{cm}^{-1} + 0.0112(v_t'+0.5)\ \text{cm}^{-1}. \tag{12}$$

However, the uncertainties of unperturbed $1\,^3\Pi_0$ level energies derived in this manner are sufficiently large [as much as $1\ \text{cm}^{-1}$ (Ref. 28)] that these values cannot be used in the determination of the energy shifts $\delta$ and $\Delta$.

Alternatively, it can be seen from Eq. (11) that the spin–orbit matrix element can also be obtained from measurements of $\delta$ and the amplitude ratio $A/B$. The latter is related to the ratio of bound–bound $2\,^1\Sigma^+ \rightarrow 1\,^1\Sigma^+$ emission to bound–free $1\,^3\Pi_0 \rightarrow 1\,^3\Sigma^+$ emission intensities from a particular perturbed level. For example, for state $\phi_2$ defined by Eq. (7)

$$\left[\frac{I_{\text{triplet}}}{I_{\text{singlet}}}\right]_2 = \frac{\epsilon_t}{\epsilon_s}\frac{\tau_s}{\tau_t}\frac{|A|^2}{|B|^2}. \tag{13}$$

Here $(\tau_s)^{-1}$ and $(\tau_t)^{-1}$ are the natural radiative rates (Einstein $A$ coefficients) of the unperturbed singlet and triplet components, respectively, and $\epsilon_s$ and $\epsilon_t$ are detection system efficiencies which incorporate collection solid angles, wavelength- and polarization-dependent monochromator (or interference filter) and detector response functions, bandpass of the monochromator (or interference filters), etc.

For the other member of the perturbed pair, $\phi_1$ [see Eq. (6)], we find

$$\left[\frac{I_{\text{triplet}}}{I_{\text{singlet}}}\right]_1 = \frac{\epsilon_t}{\epsilon_s}\frac{\tau_s}{\tau_t}\frac{|B|^2}{|A|^2}. \tag{14}$$

Therefore by measuring the energy shift $\delta$ and the ratio of triplet-to-singlet fluorescence intensities for both members of a perturbed pair, we can determine $|H_{so}|$ from

$$|H_{so}| = \delta\frac{A}{B} = \delta\left(\frac{(I_t/I_s)_2}{(I_t/I_s)_1}\right)^{1/4} = \delta\left(\frac{(I_t)_2/(I_t)_1}{(I_s)_2/(I_s)_1}\right)^{1/4}. \tag{15}$$

TABLE I. Rotational mixing coefficients for the "unperturbed" $1\,^3\Pi_0$ levels $[a'|1\,^3\Pi_0(v_t',J')\rangle + b'|1\,^3\Pi_1(v_t',J')\rangle + c'|1\,^3\Pi_2(v_t',J')\rangle]$ of NaK studied in this work.

| $1\,^3\Pi_0(v_t',J')$ | $a'$ | $b'$ | $c'$ |
|---|---|---|---|
| $1\,^3\Pi_0(23,34)$ | 0.9666 | 0.2539 | 0.0337 |
| $1\,^3\Pi_0(21,31)$ | 0.9712 | 0.2367 | 0.0292 |
| $1\,^3\Pi_0(19,28)$ | 0.9756 | 0.2183 | 0.0247 |
| $1\,^3\Pi_0(18,45)$ | 0.9444 | 0.3240 | 0.0562 |
| $1\,^3\Pi_0(17,26)$ | 0.9783 | 0.2060 | 0.0219 |

## Rotational mixing correction

As stated above, the measured values of $|H_{so}|$ must be corrected slightly to account for rotational mixing within the $^3\Pi_\Omega$ manifold. This rotational mixing causes the "unperturbed" $^3\Pi_0$ level to contain a small admixture of $^3\Pi_1$ and $^3\Pi_2$ character. One can approximately calculate these mixing coefficients by diagonalizing a $3\times3$ matrix,

$$\begin{pmatrix} H_{00}-E & H_{01} & H_{02} \\ H_{10} & H_{11}-E & H_{12} \\ H_{20} & H_{21} & H_{22}-E \end{pmatrix}\begin{pmatrix} a' \\ b' \\ c' \end{pmatrix} = \mathbf{0}, \tag{16}$$

whose matrix elements are given by Katô, Otani, and Baba,[19]

$$\begin{aligned}
H_{00} &= \langle {}^3\Pi_0|H|{}^3\Pi_0\rangle \\
&= T_v - A_v + B_v(X+1) - D_v(X^2+4X+1), \\
H_{11} &= \langle {}^3\Pi_1|H|{}^3\Pi_1\rangle = T_v + B_v(X+1) - D_v(X^2+6X-3), \\
H_{22} &= \langle {}^3\Pi_2|H|{}^3\Pi_2\rangle \\
&= T_v + A_v + B_v(X-3) - D_v(X^2-4X+5), \\
H_{01} &= H_{10} = \langle {}^3\Pi_0|H|{}^3\Pi_1\rangle = (2X)^{1/2}[B_v - 2D_v(X+1)], \\
H_{02} &= H_{20} = \langle {}^3\Pi_0|H|{}^3\Pi_2\rangle = -2D_v(X^2-2X)^{1/2}, \\
H_{12} &= H_{21} = \langle {}^3\Pi_1|H|{}^3\Pi_2\rangle = (2X-4)^{1/2}[B_v - 2D_v(X-1)].
\end{aligned} \tag{17}$$

Here $T_v = T_e + G_v$, $X = J(J+1)$, and $T_e$, $G_v$, $B_v$, $D_v$ and $A_v$ have their usual spectroscopic meanings [$A_v = A_e + \alpha_A(v+1/2)$ and $A_e$ is the $^3\Pi_\Omega$ state spin-orbit coupling constant]. Higher-order terms involving centrifugal distortion constants ($H_v$,$L_v$) have been neglected.

The measured perturbation strength $|H_{so}|_{\text{meas}}$ is related to the true $2\,^1\Sigma^+$–$1\,^3\Pi_0$ spin–orbit perturbation strength $|H_{so}|$ by the following relation:

$$\begin{aligned}
|H_{so}|_{\text{meas}} &= |\langle 2\,^1\Sigma^+(v_s',J')|\hat{H}_{so}|a'\,{}^3\Pi_0(v_t',J') \\
&\quad + b'\,{}^3\Pi_1(v_t',J') + c'\,{}^3\Pi_2(v_t',J')\rangle| \\
&= |a'|\,|H_{so}|.
\end{aligned} \tag{18}$$

Thus we must divide each measured value, $|H_{so}|_{\text{meas}}$, by the mixing coefficient $|a'|$. The $3\times3$ $^3\Pi_\Omega$ matrix [Eqs. (16) and (17)] was diagonalized for each of the five "un-



Downloaded 27 Feb 2001 to 128.180.23.36. Redistribution subject to AIP copyright, see http://ojps.aip.org/jcpo/jcpcpyrts.html

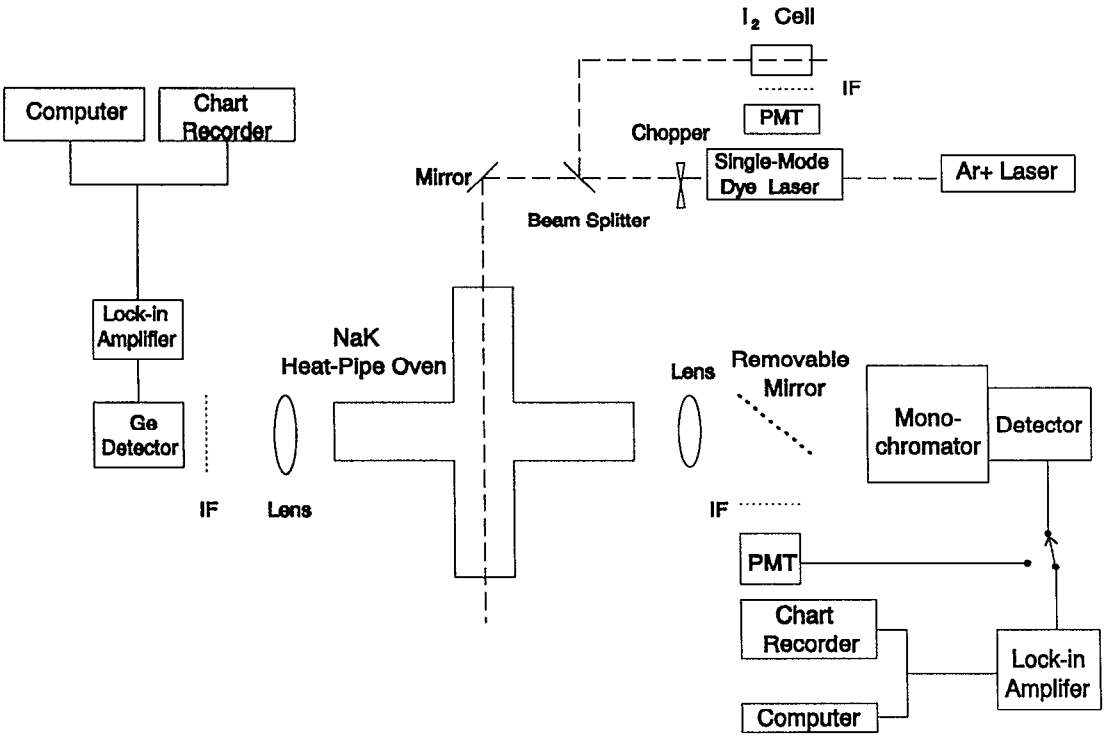


FIG. 3. Experimental setup. IF and PMT represent the interference filter and photomultiplier tube, respectively.

perturbed" $^3\Pi_0$ levels studied in this work, and the mixing coefficients $a'$, $b'$, and $c'$ were determined. These are listed in Table I.

## III. EXPERIMENTAL SETUP

The experimental setup is shown in Fig. 3. Since a setup very similar to this has already been described in detail in Ref. 23, we will only present a brief sketch of it here. The sodium–potassium mixture is contained in a stainless-steel, five-arm, crossed, heat-pipe oven.[29] The oven is operated at about 360 °C with approximately 1.5 Torr of argon as a buffer gas. A single-mode ring dye laser with built in wave meter (Coherent Autoscan CR-699-29) is used for the excitation of NaK molecules. The ring laser, using LDS 722 (pyradine 2) dye, is pumped by the 514 nm line of an argon-ion laser (7.5 W). This gives the dye laser a tuning range of 700–780 nm with between 150 and 300 mW power. The bandwidth of the ring dye laser is about 750 kHz. To check the accuracy of the wave meter on extended laser frequency scans (i.e., $\sim 10$ cm$^{-1}$), and to provide absolute calibration, part of the laser beam is split off and sent through an iodine cell. $I_2$ transitions are then calibrated against a standard reference atlas.[30,31]

Fluorescence is observed at right angles to the laser beam. Excitation spectra, in which we record total singlet emission (in the range 600 nm–1.0 $\mu$m) and total triplet emission (1.1–1.6 $\mu$m) as a function of scanned laser frequency or wavelength, are taken with the removable mirror in place (see Fig. 3). In this configuration, fluorescence is sent through the two interference filters (with 600 nm–1.0 $\mu$m and 1.1–1.6 $\mu$m transmission windows) and onto the free-standing photomultiplier and liquid-nitrogen-cooled, intrinsic germanium detector, which record total singlet and total triplet emissions, respectively. These scans are referred to as excitation scans.

Alternatively, the laser can be locked to a specific rovibrational transition, and spectrally resolved fluorescence can be recorded. In this configuration, the removable mirror is withdrawn (see Fig. 3) and singlet or triplet fluorescence is spectrally resolved using a 0.5 m monochromator. For triplet fluorescence, the monochromator slits are set to 1.5 mm (giving a spectral resolution of $\sim 2.3$ nm) and a

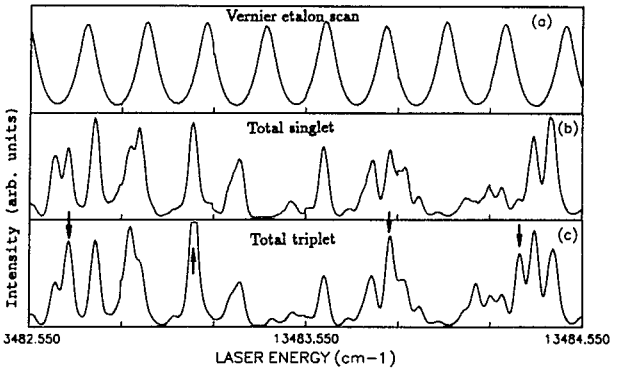


FIG. 4. Excitation spectrum. (a) The laser vernier étalon signal which demonstrates continuity of the laser frequency scan, (b) total singlet, and (c) total triplet excitation spectra, obtained as described in the text. The arrows in (c) show four frequencies where a large triplet-to-singlet intensity ratio is observed. Such positions are likely to mark mixed levels with relatively large triplet amplitudes. The oven temperature was 360 °C for this scan. The argon buffer gas pressure was 1.5 Torr.



Downloaded 27 Feb 2001 to 128.180.23.36. Redistribution subject to AIP copyright, see http://ojps.aip.org/jcpo/jcpcpyrts.html

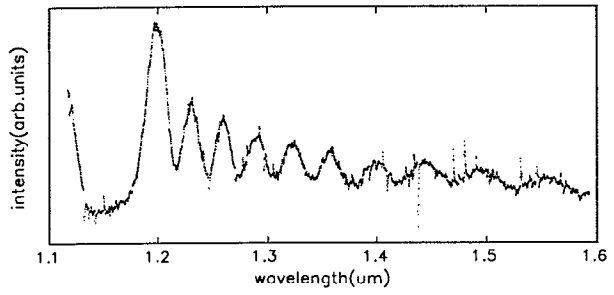


FIG. 5. Bound–free $1\,^3\Pi_0(v'_t = 18, J' = 45) \rightarrow 1\,^3\Sigma^+$ oscillatory continuum in the near infrared. The laser was tuned to 13 572.006 $cm^{-1}$, pumping the $[1\,^3\Pi_0(v'_t = 18, J' = 45)$–$2\,^1\Sigma^+(v'_s = 20, J' = 45)] \leftarrow 1\,^1\Sigma^+(v'' = 0, J'' = 46)$ transition. $T = 360$ °C. $P_{Ar} = 1.5$ Torr. Sharp spikes on the spectrum are due to cosmic rays to which the Ge detector is sensitive.

second intrinsic Ge detector is mounted to receive the transmitted light. For singlet fluorescence, a photomultiplier tube (PMT) (either Hamamatsu R928 or R406) is mounted on the monochromator, and the slits are set to 50–70 $\mu$m, giving a resolution of better than $\sim 1$ Å. This resolution is necessary to distinguish individual rovibrational transitions originating from neighboring levels.

## IV. EXPERIMENTAL PROCEDURE

The step-by-step procedure we used for identifying both members of a mutually perturbing pair and for measuring the energy splittings and singlet and triplet conponent amplitudes is given below. We note that the cumbersome nature of this procedure is a result of the availability of only one single-frequency laser. With two such lasers, state-labeling techniques could have been used, which would have allowed rapid identification of both members of the pair.

### A. Finding the first member of a mutually perturbing pair

The technique of finding a good candidate for a well-mixed $1\,^3\Pi_0$–$2\,^1\Sigma^+$ level involves the monitoring of total laser-induced singlet and triplet band fluorescence. Since the emission wavelengths of the $2\,^1\Sigma^+ \rightarrow 1\,^1\Sigma^+$ and $1\,^3\Pi_0 \rightarrow 1\,^3\Sigma^+$ bands are well separated, we are able to observe the total fluorescence of each band individually with the use of interference filters. Figure 4 shows an example of an excitation spectrum taken as a function of laser frequency. The spectrum consists of a vernier étalon scan (which shows continuity of the laser frequency scan), a total singlet fluorescence scan, and a total triplet fluorescence scan.

In the excitation spectra, the total triplet fluorescence trace follows the total singlet, nearly peak for peak, because collisions can transfer population from the laser-pumped $2\,^1\Sigma^+$ levels to nearby rovibrational levels of the $1\,^3\Pi_\Omega$ states. However, there are a few peaks showing an enhancement of total triplet fluorescence relative to total singlet fluorescence. These are likely candidates for mixed levels with large triplet amplitudes. We therefore fix the laser frequency at some of these enhanced triplet emission

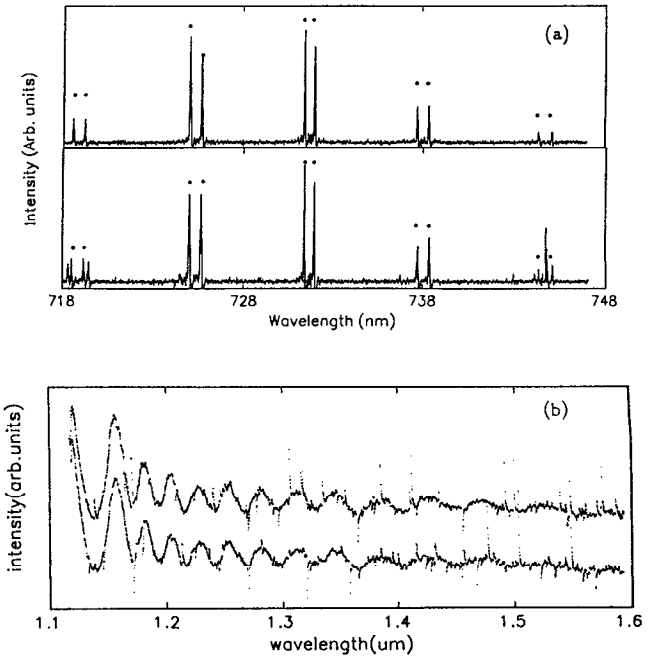


FIG. 6. Laser-induced fluorescence. (a) Bound–bound singlet laser-induced fluorescence spectra generated when the same upper mixed level [one level of the $1\,^3\Pi_0(v'_t = 21, J' = 31)$–$2\,^1\Sigma^+(v'_s = 24, J' = 31)$ mutually perturbing pair] is pumped with $R$ line excitation from the $1\,^1\Sigma^+(v'' = 1, J'' = 30)$ level with the laser tuned to 13 787.742 $cm^{-1}$ (upper panel), and by $P$ line excitation from the $1\,^1\Sigma^+(v'' = 1, J'' = 32)$ level with the laser tuned to 13 775.886 $cm^{-1}$ (lower panel). Note that in addition to the primary series of interest (marked by **), members of unrelated series, resulting from accidental pumping of other transitions which happen to overlap the laser frequency within their Doppler widths, are also sometimes present. However, the assignment of $v'_s$, $J'$ is confirmed by identifying the same ** series (including the same relative amplitudes) in both spectra. Note: Only short segments of the spectra are shown here. However, this ** series can be followed out to $\sim 1$ $\mu$m, and all such peaks match up in the two spectra. (b) Triplet spectra corresponding to pumping the same $R$ line (upper trace) and $P$ line (lower trace) as in (a). Again, the continuum oscillations must line up if the assignment is correct.

positions and record-resolved $1\,^3\Pi_0 \rightarrow 1\,^3\Sigma^+$ spectra (fluorescence spectra obtained using the monochromator in Fig. 3). The triplet spectrum from a strongly perturbed level will consist of a well-developed oscillatory continuum (see Fig. 5), which is characteristic of bound–free reflection structure (see Ref. 32). For cases where the triplet emission results primarily from singlet-to-triplet collisional excitation transfer, the oscillatory structure is largely washed out.

### B. Determination of the unperturbed energy of the $2\,^1\Sigma^+(v'_s, J')$ component of a mixed level

In order to determine the line shifts $\delta$ and $\Delta$, we must first calculate the energy of the unperturbed singlet component. To do the latter, we must identify the vibrational and rotational quantum numbers ($v'_s$ and $J'$) of the singlet component for the particular mixed $2\,^1\Sigma^+(v'_s, J')$–$1\,^3\Pi_0(v'_t, J')$ level ($\phi_1$ or $\phi_2$). We therefore record the resolved singlet fluorescence spectrum with the laser tuned to pump the mixed level of interest. The singlet



Downloaded 27 Feb 2001 to 128.180.23.36. Redistribution subject to AIP copyright, see http://ojps.aip.org/jcpo/jcpcpyrts.html

spectrum consists of a series of $P$–$R$ doublets, $2\,^1\Sigma^+(v_s',J') \rightarrow 1\,^1\Sigma^+(v'',J'' = J' \pm 1)$, obeying the $\Delta J = \pm 1$ selection rule appropriate for a $\Sigma \rightarrow \Sigma$ transition. The upper panel of Fig. 6(a) shows part of one of these resolved singlet spectra.

The analysis of such a spectrum yields $v_s'$ and $J'$ since the splitting between doublets depends primarily on $v''$ while the $P$–$R$ line splittings within each doublet depend primarily on $J'$. These identifications are made by comparison to a list of $1\,^1\Sigma^+$ state rovibrational level energies generated from the experimental constants of Ref. 25. Combining the lower state assignments with the known laser frequency determines $v_s'$ with no uncertainty. However, due to the resolution of the monochromator, the assignment of $J'$ has an uncertainty of approximately $\pm 2$. Therefore we calculate

$$\Delta E(v'',J' \pm 1) \equiv E(1\,^1\Sigma^+(v'',J''=J'+1)) - E(1\,^1\Sigma^+(v'',J''=J'-1)) \qquad (19)$$

from the experimental constants of Ross *et al.*[25] for each of the possible values of $J'$ determined from the monochromator scans. We shift the laser frequency by $\Delta E(v'',J' \pm 1)$ for each of these possible $J'$ values and look at the resolved singlet spectra that are generated. For the correct assignment of $J'$, the shift of $\Delta E(v'',J' \pm 1)$ will result in pumping the same upper state (i.e., if we initially pump $R_{J'-1}$ then the shift will cause us to pump $P_{J'+1}$ and vice versa). Thus when the assignment is correct, we observe the same resolved singlet [see Fig. 6(a)] and triplet [Fig. 6(b)] spectra for both $P$ and $R$ excitation of the same upper mixed level.

Once the assignments of $v_s'$ and $J'$ are confirmed, $E_\Sigma^0[2\,^1\Sigma^+(v_s',J')]$ can be calculated from the exprimental constants of Ref. 26.

### C. Finding the second level of a mutually perturbing pair

Next, we must find the other perturbed level, shifted by $|E_+ - E_-|$ (between 0.5–6 $cm^{-1}$ for the five perturbed pairs studied in this work) from the first. This is not easy since there are hundreds of unrelated lines between the transitions to $E_+$ and $E_-$.

It is well known that the energy shifts of both perturbed levels from their unperturbed positions are "repulsive;" i.e., the higher unperturbed level is displaced upward and the lower is displaced downward by the same amount[20] (see Fig. 2). Therefore we can estimate the position of the second member of the perturbed pair from the position of the first one and the accurately known unperturbed energy $E_\Sigma^0$. If the energy of the first level is greater than $E_\Sigma^0$, we have found $E_+$. Otherwise we have found $E_-$ (see Fig. 2). In either case, the difference $|E_\pm - E_\Sigma^0|$ is equal to either $\delta$ or $\Delta$. Thus the other member of the perturbed pair is separated from the first by

$$E_+ - E_- = 2\delta + |E_\Sigma^0 - E_\Pi^0| = 2\Delta - |E_\Sigma^0 - E_\Pi^0|, \qquad (20)$$

which can be calculated roughly from the accurate $E_\Sigma^0$ values of Ref. 26 and the approximate $E_\Pi^0$ values from Ref. 24.

Depending on whether our first measurement yielded $\delta$ (i.e., if we found the "perturbed singlet," defined as the level with singlet amplitude greater than triplet amplitude) or $\Delta$ (if we found the "perturbed triplet") we can narrow the search to either one of two smaller ranges. Most often, we first find the perturbed triplet (since we pick out peaks with large triplet amplitudes), so we begin our search in the region shifted by $(2\Delta - |E_\Sigma^0 - E_\Pi^0|)$.

The keys to finding the correct level in this region (since the total number of transitions to choose from is still large) are as follows:

(1) The other member of the perturbed pair will give

TABLE II. Experimental measurements of the energies (relative to the bottom of the ground-state well) of mutually perturbing pairs of NaK $2\,^1\Sigma^+(v_s',J')$ and $1\,^3\Pi_0(v_t',J')$ levels, and the ratios of triplet-to-singlet emission intensities.

| Excitation $2\,^1\Sigma^+(v_s',J')$–$1\,^3\Pi_0(v_t',J')$ $\leftarrow 1\,^1\Sigma^+(v'',J'')$ | $E^0(2\,^1\Sigma^+)$ ($cm^{-1}$) | $E_+$($cm^{-1}$) | $E_-$($cm^{-1}$) | $\frac{(I_t/I_s)_2}{(I_t/I_s)_1}$ |
|---|---|---|---|---|
| $2\,^1\Sigma^+(27,34)$–$1\,^3\Pi_0(23,34)$ $\leftarrow 1\,^1\Sigma^+(2,33)$ | 14 285.4775 | 14 286.502 | 14 284.675 | 1.566 |
| $2\,^1\Sigma^+(24,31)$–$1\,^3\Pi_0(21,31)$ $\leftarrow 1\,^1\Sigma^+(1,30)$ | 14 060.5476 | 14 060.961 | 14 060.386 | 7.109 |
| $2\,^1\Sigma^+(21,28)$–$1\,^3\Pi_0(19,28)$ $\leftarrow 1\,^1\Sigma^+(0,27)$ | 13 833.5357 | 13 835.338 | 13 832.251 | 1.456 |
| $2\,^1\Sigma^+(20,45)$–$1\,^3\Pi_0(18,45)$ $\leftarrow 1\,^1\Sigma^+(0,46)$ | 13 835.4795 | 13 838.224 | 13 833.722 | 1.512 |
| $2\,^1\Sigma^+(18,26)$–$1\,^3\Pi_0(17,26)$ $\leftarrow 1\,^1\Sigma^+(0,25)$ | 13 607.5995 | 13 611.582 | 13 606.232 | 3.582 |



Downloaded 27 Feb 2001 to 128.180.23.36. Redistribution subject to AIP copyright, see http://ojps.aip.org/jcpo/jcpcpyrts.html

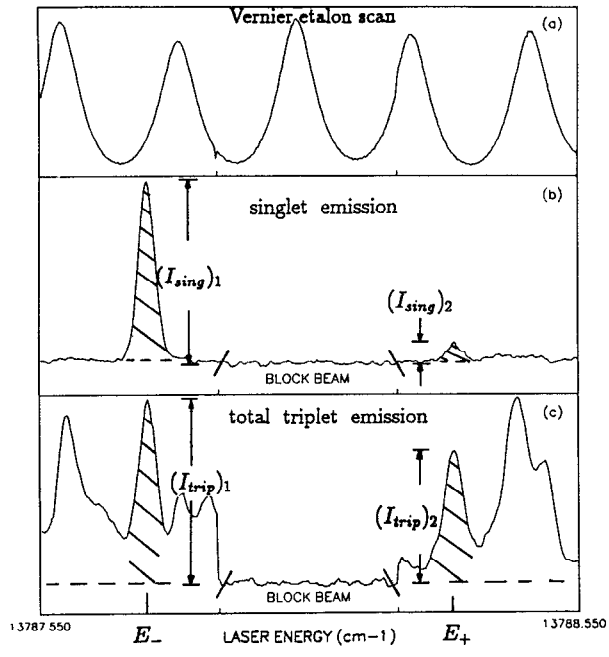


FIG. 7. Intensity measurements for the perturbed pair ($E_+$ = 14 060.961 cm$^{-1}$ and $E_-$ = 14 060.386 cm$^{-1}$). The singlet excitation spectrum was taken by scanning the laser while monitoring the bound–bound 2 $^1\Sigma^+(v_s' = 24, J' = 31) \rightarrow 1\ ^1\Sigma^+(v'' = 2, J'' = 30)$ transition. The total triplet excitation spectrum was measured simultaneously. The base line was obtained by blocking the laser (region between the /\slash marks).

an identical resolved singlet spectrum (including relative line intensities) as the first, but all lines will be shifted by $\delta + \Delta$.

(2) The other member of the perturbed pair will give an identical resolved triplet spectrum as the first.

(3) If the first transition we pumped was an $R$ ($P$) line $2\ ^1\Sigma^+(v_s', J') \leftarrow 1\ ^1\Sigma^+(v'', J' - 1)$ [$2\ ^1\Sigma^+(v_s', J') \leftarrow 1\ ^1\Sigma^+(v'', J' + 1)$], the transition to the second member of the perturbed pair found in this manner must also be an $R$ ($P$) line since the method is based on the splitting between upper states assuming pumping from the same lower state.

(4) Once found, a shift of the laser frequency by $\Delta E(v'', J' \pm 1)$ [Eq. (19)] switches from $R$ to $P$ (or $P$ to $R$) line pumping of this second perturbed upper level and must therefore produce the same singlet and triplet spectra.

To carry out this procedure we set the monochromator slits to give a resolution no better than twice the expected energy difference ($E_+ - E_-$) and the monochromator transmission wavelength to one of the lines in the resolved singlet spectrum of the first perturbed level. The laser is scanned in the range where the transition to the second member is predicted to lie, and an excitation scan (for producing emission within the monochromator bandwidth) is recorded. Generally, in the resulting excitation spectrum there is still a fairly large number of lines. We then set the monochromator wavelength to the position of another line in the first level's resolved singlet spectrum and again record the excitation scan. After recording scans for several such monochromator wavelength settings, we look for lines that appear in all of them, eliminating those with intensities for $P$–$R$ fluorescence doublets which are not comparable. For each of the remaining transitions (5–10 lines in an $\sim 5$ cm$^{-1}$ range) we must record complete resolved singlet and/or triplet spectra using both $P$ and $R$ line pumping. The two members of the same perturbed pair, with both $P$ and $R$ line pumping, yield the same resolved singlet and resolved triplet spectra. Our experimental measurements of $E_+$ and $E_-$ are listed in Table II for the five pairs studied. These energies are all referenced to the bottom of the $1\ ^1\Sigma^+$ well (i.e., they are the calibrated laser excitation energies added to the energy of the lower level of the transition, which is computed from the constants of Ref. 25).

TABLE III. Parameters for $2\ ^1\Sigma^+$–$1\ ^3\Pi_0$ spin–orbit perturbations in NaK. The subscripts $s$ and $t$ represent values obtained from shift and intensity measurements, respectively. Values of $H_{so}$ and $H_{el}$ have been corrected for the $1\ ^3\Pi_\Omega$ rotational mixing effects. Values in parentheses indicate uncertainties.

| Excitation $2\ ^1\Sigma^+(v_s', J')$–$1\ ^3\Pi_0(v_t', J')$ $\leftarrow 1\ ^1\Sigma^+(v'', J'')$ | $A^2$ | $B^2$ | $(H_{so})_s$ (cm$^{-1}$) | $(H_{so})_t$ (cm$^{-1}$) | $\lvert\langle v_s' \rvert v_t' \rangle\rvert$ | $(H_{el})_s$ (cm$^{-1}$) | $(H_{el})_t$ (cm$^{-1}$) |
|---|---|---|---|---|---|---|---|
| $2\ ^1\Sigma^+(27,34)$–$1\ ^3\Pi_0(23,34)$ $\leftarrow 1\ ^1\Sigma^+(2,33)$ | 0.56 | 0.44 | 0.9381 | 0.9291 | 0.057 36 | 16.36 (1.59) | 16.20 (3.43) |
| $2\ ^1\Sigma^+(24,31)$–$1\ ^3\Pi_0(21,31)$ $\leftarrow 1\ ^1\Sigma^+(1,30)$ | 0.72 | 0.28 | 0.2663 | 0.2720 | 0.016 14 | 16.50 (6.67) | 16.86 (12.76) |
| $2\ ^1\Sigma^+(21,28)$–$1\ ^3\Pi_0(19,28)$ $\leftarrow 1\ ^1\Sigma^+(0,27)$ | 0.58 | 0.42 | 1.5597 | 1.4463 | 0.098 03 | 15.91 (0.93) | 14.75 (2.59) |
| $2\ ^1\Sigma^+(20,45)$–$1\ ^3\Pi_0(18,45)$ $\leftarrow 1\ ^1\Sigma^+(0,46)$ | 0.61 | 0.39 | 2.3254 | 2.0633 | 0.1463 | 15.89 (0.66) | 14.10 (2.44) |
| $2\ ^1\Sigma^+(18,26)$–$1\ ^3\Pi_0(17,26)$ $\leftarrow 1\ ^1\Sigma^+(0,25)$ | 0.74 | 0.26 | 2.3856 | 1.9235 | 0.1507 | 15.83 (0.75) | 12.82 (1.54) |



Downloaded 27 Feb 2001 to 128.180.23.36. Redistribution subject to AIP copyright, see http://ojps.aip.org/jcpo/jcpcpyrts.html

### D. Intensity measurements

With laser pumping of each member of a perturbed pair, we simultaneously measure the triplet and singlet fluorescence intensities. The experimentally measured resolved triplet spectra, from all levels studied here, show well-developed oscillatory structures, indicating that these emissions are predominantly direct rather than collision induced. Therefore we monitor total triplet emission from these perturbed levels by the free-standing Ge detector as described above. On the other hand, some of the resolved singlet spectra show additional lines, unrelated to the perturbed levels, which result from accidental pumping of other transitions. We therefore monitor the singlet intensity using the monochromator set to a particular $P$ or $R$ line of the perturbed level fluorescence spectrum. Figure 7 shows intensity measurements for one perturbed pair. The experimental results of these intensity measurements, for our five observed perturbed pairs, are listed in Table II. Due to uncertainty in base lines caused by overlapping lines (see Fig. 7), and from collisional contributions to the triplet emissions, these results carry considerable uncertainties.

## V. RESULTS AND DISCUSSION

The values of the perturbation matrix elements, $|H_{so}|$, were determined from our measurements for these five observed perturbed pairs and are given in Table III. $(H_{so})_s$ denotes the values of $|H_{so}|$ obtained from the energy shifts $\delta$ and $\Delta$ and Eq. (10). Similarly, $(H_{so})_I$ denotes values obtained from the shift $\delta$, the amplitude ratio $A/B$, and Eq. (15). In both cases these values have been corrected for the $^3\Pi_\Omega$ rotational coupling effect discussed in Sec. II; i.e., the measured values of $|H_{so}|_{meas}$ have been divided by the rotational mixing coefficient $|a'|$ listed in Table I. This correction is typically 2%–5%.

The spin–orbit operator acts primarily on the electronic part of the wave functions. Thus we can factor the full singlet and triplet wave functions into products of electronic, vibrational, and rotational terms. We can then define a quantity,

$$H_{el}=\frac{|\langle 1\,^3\Pi_0(v_t',J')|\hat{H}_{so}|2\,^1\Sigma^+(v_s',J')\rangle|}{|\langle v_t'|v_s'\rangle|}, \qquad (21)$$

which only depends on the electronic wave functions so long as the spin–orbit matrix element is roughly independent of $R$ over the range of overlap of the two wave functions.[14,16,19] To obtain the vibrational overlap integrals $\langle v_t'|v_s'\rangle$ we constructed Rydberg–Klein–Rees potential curves for the $2\,^1\Sigma^+$ and $1\,^3\Pi_0$ states using the constants of Refs. 26 and 24, respectively. We then numerically solved the radial Schrödinger equation for these potentials and numerically integrated the product of the resulting vibrational wave functions.

Under these conditions, $H_{el}$, the electronic part of the spin–orbit perturbation matrix element, is expected to depend only on the two electronic states and not on the specific $v_s'$, $v_t'$, and $J'$ values. Our results for $H_{el}$, obtained from both the shift and intensity methods, for each of the five perturbed pairs studied, are given in Table III. Although the intensity results are less accurate, all of these values are consistent, as expected.

TABLE IV. Spin–orbit coupling constant for the $1\,^3\Pi_\Omega$ levels ($A_e$) and the electronic part of the $A\,^1\Sigma^+$–$1\,^3\Pi_0$ spin–orbit perturbation strength ($H_{el}$) for alkali diatomic molecules.

| Molecule | $A_e$ (cm$^{-1}$) | $H_{el}$ (cm$^{-1}$) |
|---|---|---|
| $Li_2$ | ··· | 0.114±0.006[a] |
| $Na_2$ | 7.08[b] | 5.91±0.14[b] |
| NaK | 15.56[c] | 15.64±0.39[d] |
| $K_2$ | 21.5[e] | 18.4±0.2[e] |

[a]Reference 4.
[b]Reference 16.
[c]Reference 24.
[d]This work.
[e]Reference 18.

$E_+$ and $E_-$ can be measured with high precision using the single-mode laser and wave meter. However, the uncertainty in the unperturbed singlet energy levels $E^0(2\,^1\Sigma^+)$ is estimated to be $\sim$0.12 cm$^{-1}$ (see Ref. 26). Thus the small shifts $\delta$ and $\Delta$ can also be uncertain by that amount. If the shift is small (as for our second entry in Tables II and III), the uncertainty in $E^0(2\,^1\Sigma^+)$ will dominate the overall uncertainty in $H_{el}$. The other significant source of uncertainty in the $H_{el}$ values determined by the energy shift method is the uncertainty in the vibrational overlap integral $\langle v_t'|v_s'\rangle$. This latter uncertainty is primarily due to uncertainty in our knowledge of the $1\,^3\Pi_0$ potential well. The uncertainty of the $H_{el}$ values determined from the intensity measurements (combined with the shift $\delta$) comes not only from the uncertainties in $\delta$ and $\langle v_t'|v_s'\rangle$, but also from uncertainties in the singlet and triplet emission intensity measurements. The latter is particularly large due to triplet emission resulting from collisional transfer. In both cases, the $1\,^3\Pi_\Omega$ rotational mixing corrections are only a few percent. Thus the manner in which this correction was included is not expected to affect our results significantly. In this context, it should be noted that the "correct" way to deal with this rotational mixing effect is to diagonalize the full 4×4 matrix. However, in the present case, this was not possible since the unperturbed $1\,^3\Pi_2$ and $1\,^3\Pi_0$ energies are not known with sufficient accuracy. As a test of our method for including the rotational mixing effect, we have analyzed the results for sodium presented in Ref. 19 using this method (i.e., first solving the $b\,^3\Pi_0$–$A\,^1\Sigma^+$ 2×2 matrix and then introducing the rotational mixing correction as described in Sec. II), and found that values of $H_{el}$ we obtained agree extremely well with values found from the 4×4 matrix analysis in that work. Note also that the present method does not depend critically on knowledge of the unperturbed $1\,^3\Pi_0$ and $1\,^3\Pi_2$ energies since the full rotational mixing correction only changes the value of $H_{el}$ by a few percent.

Estimated uncertainties in $(H_{el})_s$ and $(H_{el})_I$ are given in Table III. From the weighted mean of the ten measured values of $H_{el}$ we find the best value of

$$H_{el}=(15.64\pm0.39)\ \text{cm}^{-1}. \qquad (22)$$


Downloaded 27 Feb 2001 to 128.180.23.36. Redistribution subject to AIP copyright, see http://ojps.aip.org/jcpo/jcpcpyrts.html

Table IV gives a comparison of measured $A\,^1\Sigma^+$–$1\,^3\Pi_0$ $H_{el}$ values for various alkali diatomic molecules. It can be seen that the value for NaK lies between those for $Na_2$ and $K_2$, as expected. It is also reasonable to expect that $H_{el}$ for NaK would lie closer to the value for $K_2$ than to the value for $Na_2$, since the $A(2)\,^1\Sigma^+$ and $b(1)\,^3\Pi$ states of NaK both dissociate to the Na($3s$) +K($4p$) atomic limit. This idea is also in agreement with the present results. However, we note (see Table IV) that while the values of $H_{el}$ for $Na_2$ and $K_2$ are approximately 85% of $A_e$ for those molecules (where $A_e$ is the spin–orbit coupling constant for the $1\,^3\Pi_\Omega$ levels), our value of $H_{el}$ for NaK is 101% of the corresponding $A_e$ value. At present, we do not understand the origin of this difference, although it may be partly explained by uncertainty in the approximate $A_e$ value reported in Ref. 24.

## ACKNOWLEDGMENTS

We thank Dr. Mark Masters and Dr. Marjatta Lyyra for many stimulating and helpful discussions, and Dr. Ken Sando for providing many of the computer programs used in this analysis. We are grateful to the referee for suggesting that we consider the effects of the $1\,^3\Pi_\Omega$ rotational mixing corrections, and we are deeply indebted to Dr. Mingguang Li for several illuminating discussions which helped us to understand these corrections, as well as several other important points. We gratefully acknowledge the U.S. Army Research Office (Grant No. DAAL03-89-K-0171) and the National Science Foundation (Grant No. PHY-9119498) for their generous support of this work.

[1] K. K. Verma, J. T. Bahns, A. R. Rajaei-Rizi, W. C. Stwalley, and W. T. Zemke, J. Chem. Phys. **78**, 3599 (1983).
[2] C. Amiot, W. Demtröder, and C. R. Vidal, J. Chem. Phys. **88**, 5265 (1988).
[3] L. Li and R. W. Field, J. Phys. Chem. **87**, 3020 (1983).
[4] Xingbin Xie and R. W. Field, Chem. Phys. **99**, 337 (1985).
[5] Xingbin Xie and R. W. Field, J. Mol. Spectrosc. **117**, 228 (1986).
[6] D. D. Konowalow and P. S. Julienne, J. Chem. Phys. **72**, 5815 (1980).
[7] A. Gallagher and D. E. Pritchard, Phys. Rev. Lett. **63**, 957 (1989).
[8] D. Sesko, T. Walker, C. Monroe, A. Gallagher, and C. Wieman, Phys. Rev. Lett. **63**, 961 (1989).
[9] P. S. Julienne and J. Vigué, Phys. Rev. A **44**, 4464 (1991).
[10] W. R. Fredrickson and C. R. Stannard, Phys. Rev. **44**, 632 (1933).
[11] T. Carroll, Phys. Rev. **52**, 822 (1937).
[12] P. Kusch and M. M. Hessel, J. Chem. Phys. **63**, 4087 (1975).
[13] J. B. Atkinson, J. Becker, and W. Demtröder, Chem. Phys. Lett. **87**, 92 (1982).
[14] F. Engelke, H. Hage, and C. D. Caldwell, Chem. Phys. **64**, 221 (1982).
[15] K. Shimizu and F. Shimizu, J. Chem. Phys. **78**, 1126 (1983).
[16] C. Effantin, O. Babaky, K. Hussein, J. d'Incan, and R. F. Barrow J. Phys. B **18**, 4077 (1985).
[17] O. C. Mullins, C. R. Mahon, and T. F. Gallagher, Chem. Phys. Lett. **126**, 501 (1986).
[18] A. J. Ross, P. Crozet, C. Effantin, J. d'Incan, and R. F. Barrow, J. Phys. B **20**, 6225 (1987).
[19] H. Katô, M. Otani, and M. Baba, J. Chem. Phys. **89**, 653 (1988).
[20] G. Herzberg, *Molecular Spectra and Molecular Structure I, Spectra of Diatomic Molecules* (Van Nostrand Reinhold, New York, 1950).
[21] F. W. Loomis and M. J. Arvin, Phys. Rev. **46**, 286 (1934).
[22] J. Huennekens, A. Loza, M. Masters, and K. M. Sando, J. Chem. Phys. **88**, 6013 (1988).
[23] M. Masters, J. Huennekens, W. T. Luh, L. Li, A. M. Lyyra, K. Sando, V. Zafiropulos, and W. C. Stwalley, J. Chem. Phys. **92**, 5801 (1990).
[24] A. J. Ross, C. Effantin, J. d'Incan, and R. F. Barrow, J. Phys. B **19**, 1449 (1986).
[25] A. J. Ross, C. Effantin, J. d'Incan, and R. F. Barrow, Mol. Phys. **56**, 903 (1985).
[26] A. J. Ross, R. M. Clements, and R. F. Barrow, J. Mol. Spectrosc. **127**, 546 (1988).
[27] H. Lefebvre-Brion and R. W. Field, *Perturbations in the Spectra of Diatomic Molecules* (Academic, Orlando, 1986).
[28] A. J. Ross (private communication).
[29] C. R. Vidal and J. Cooper, J. Appl. Phys. **40**, 3370 (1969).
[30] S. Gerstenkorn, J. Vergés, and J. Cherillard, *Atlas du spectre D'Absorption de la Molecule D'Iode, 11000–14000* $cm^{-1}$ (CNRS, Paris, 1982).
[31] S. Rakowsky, D. Zimmermann, and W. E. Ernst, Appl. Phys. B **48**, 463 (1989).
[32] J. Tellinghuisen, J. Mol. Spectrosc. **103**, 455 (1984).
[33] W. J. Stevens, D. D. Konowalow, and L. B. Ratcliff, J. Chem. Phys. **80**, 1215 (1984).



Downloaded 27 Feb 2001 to 128.180.23.36. Redistribution subject to AIP copyright, see http://ojps.aip.org/jcpo/jcpcpyrts.html